# Some Recent Developments in ab initio Thermodynamics of Ion Disorder in Solids

Shusuke KASAMATSU
*Academic Assembly (Faculty of Science), Yamagata University*
*Kojirakawa, Yamagata-shi, Yamagata, JAPAN 990-8560*

## Abstract

Configurational disorder of ions in solids often play key roles in determining the properties of functional materials. A natural way to obtain thermodynamically relevant structures from the combinatorially increasing number of configurations in multicomponent systems is to combine computational statistical physics methods such as Metropolis sampling with *ab initio* methods. Since *ab initio* methods incur high computational costs, the usual approach is to fit *ab inito* datasets to low-cost models such as cluster expansion, then use those models for sampling. However, obtaining reliable low-cost models for complex oxide systems have turned out to be challenging. To circumvent this problem, we have recently been examining the feasibility of direct sampling on *ab initio* energies, as well as turning to more flexible neural network models as an alternative to cluster expansion. Here, we review some of our recent works in this direction; we also introduce our open source code *abICS*, which is designed to harness the computational capacity of modern supercomputers to perform configurational sampling on complex multicomponent systems.

## 1 Introduction

Functional materials for various applications including energy conversion, nanoelectronics devices, and structural materials exhibit varying levels of configurational disorder which depend on the details of materials processing including temperature and chemical potentials. Such disorder often plays significant roles in determining materials properties, and many materials in e.g., battery or magnet applications utilize impurities to cause disorder on purpose so as to obtain desirable properties. Thus, the ability to simulate such disorder as a function of temperature should be immensely helpful for prediction and design of properties in materials with realistic levels of disorder. To achieve this, it is necessary to perform sufficient thermodynamic sampling based on statistical mechanics. First-principles molecular dynamics is the method of choice for sampling quickly-relaxing (e.g., liquid) systems, but it is nearly useless for sampling solid state systems with very high energy barriers between different configurations. On the other hand, Monte Carlo methods are not limited by realistic relaxation time scales since they can employ "unphysical" trial steps such as swapping of atom positions. However, standard Metropolis Monte Carlo sampling can still get trapped in local minima, and it is usually not efficient enough to allow for a direct combination with first-principles calculations. Thus, many workers have opted to first derive lightweight models from first-principles calculations, then use those models for Monte Carlo sampling.

For modeling of systems that can be mapped to a lattice (i.e., crystalline systems with configurational disorder), the cluster expansion approach has seen much success [1–8]. This method expands the total energy in terms of "clusters" of

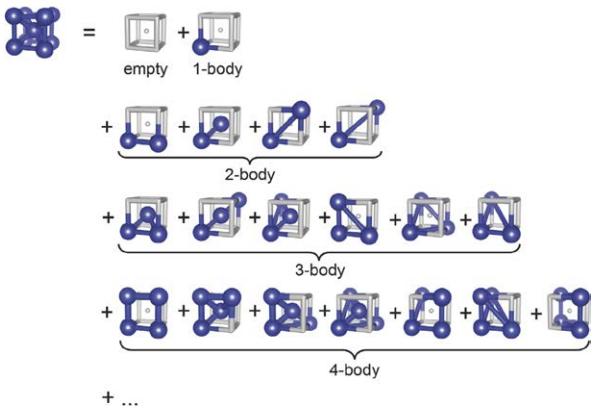


Figure 1: Clusters within the conventional BCC cell. From Chang et al. [8] (Creative Commons Attribution License 3.0, `https://doi.org/10.1088/1361-648X/ab1bbc`).

atoms (Fig. 1):

$$E(\vec{\sigma}) = \sum_{\alpha} m_\alpha V_\alpha \Phi_\alpha(\vec{\sigma}), \tag{1}$$

where $\alpha$ denotes empty, single, and multi-component clusters, $m_\alpha$ is the cluster multiplicity, and $\vec{\sigma}$ is the occupation vector. $\Phi_\alpha$ is the cluster basis function, which for a binary system takes the simple form of

$$\Phi_\alpha(\vec{\sigma}) = \prod_{p \in \alpha} \sigma_p, \tag{2}$$

where $p$ are site indices and $\sigma_p = \pm 1$ depending on which component occupies site $p$. $V_\alpha$ is the effective cluster interaction (ECI), which represents the contribution of each cluster to the total energy. This model reduces to the classical Ising model when considering only nearest neighbor pair clusters. The ECIs are usually obtained by fitting to energies of relaxed structures from many small-scale first-principles density functional theory (DFT) calculations, then used to perform Monte Carlo sampling on a larger cell.

The efficiency of the cluster expansion approach depends on the ability to quantitatively reproduce configuration energies using as few clusters (and corresponding ECIs) as possible. This is rarely an issue for simple two-component metallic alloys where considering only near-neighbor interactions often leads to sufficient accuracy. However, complex systems such as multicomponent oxides often require many clusters due to longer range coulomb interactions as well as complicated strain patterns. In addition to this, increasing the number of components (i.e., ion types) leads to a combinatorial increase in the number of clusters which makes cluster expansion computationally unfeasible. Another issue that has been recognized when using cluster expansion is that surface calculations require many more clusters than bulk calculations for sufficient accuracy [9].

There are two possible ways to tackle the above issue. One approach is to bypass the use of models and sample directly on first-principles energies. Although this approach is computationally expensive as mentioned above, the use of parallel sampling algorithms combined with modern-day supercomputers have made it just barely feasible in recent years. Another approach is to utilize recently-developed machine-learning models which is expected to be more flexible than the cluster expansion model. We have been working on both fronts; we will review some of the literature as well as our recent developments on the former approach in Sec. 2 and the latter approach in Sec. 3. A software framework that incorporates these developments, which we have named ab Initio Configuration Sampling Toolkit, or *abICS* for short, is introduced in Sec. 5.

## 2 Direct coupling of first-principles calculations with replica exchange sampling [10]

There have already been some reports of first-principles Monte Carlo simulation in the literature, but they were limited to relatively simple and quickly relaxing systems where first-principles molecular dynamics may be just as efficient [11, 12]. The issue, as noted above, is the tendency to get stuck in local minima, especially at low temperatures. One may think that with the increase in computer power available to researchers today, simply performing many Metropolis sam-

pling calculations in parallel would lead to a sufficient number of samples for obtaining statistically relevant results. However, such embarrassingly parallel sampling is useless if each parallel image cannot achieve equilibrium. The reason for getting trapped in local minima is that the Metropolis algorithm samples the canonical ensemble; a given configuration is sampled with a probability proportional to $\exp(-\beta E)$, where $\beta$ is the inverse temperature and $E$ is the energy of the configuration. Thus, configurations residing at or near energy barriers on the potential energy surface will rarely be accepted and the difficulty to cross such energy barriers increases exponentially with $\beta E$.

This is where the so-called *extended ensemble* sampling comes to the rescue. Using histogram reweighting [13], it is possible, in theory, to convert between arbitrary ensembles. Thus, we are not limited to sampling in a single canonical ensemble at a given temperature, and this allows for choosing ensembles that can avoid the minima trapping issue. For example, one can choose to sample an ensemble where each configuration is realized with probabilities proportional to the inverse of the density of states. This is the idea behind multicanonical [14] and Wang-Landau [15] methods. In fact, the Wang-Landau method was recently used successfully in combination with order-$N$ first-principles Korringa-Kohn-Rostoker approach (albeit without structural relaxation) to calculate the order-disorder transition in a 250-atom CuZn supercell [16].

On the other hand, we have been working extensively on combining first-principles calculation with another popular extended ensemble method, i.e., the replica exchange Monte Carlo (RXMC) method [17]. This approach considers an ensemble of $N_{\mathrm{rep}}$ replicas of a given system at $N_{\mathrm{rep}}$ different temperatures. Each replica is simulated in the canonical ensemble, so the low temperature replicas would still have the minima trapping issue. However, the problem is alleviated by allowing swaps of temperatures between replicas according to the following Metropolis criterion for

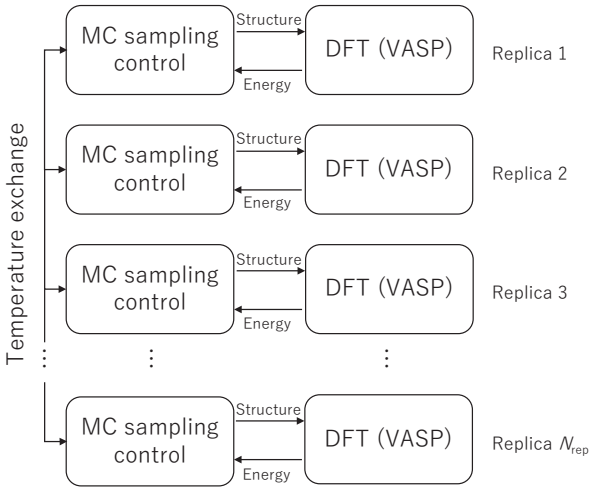


Figure 2: Schematic of our scheme for coupling the RXMC method with DFT codes. Reproduced from Ref. [10]

the ensemble of $N_{\mathrm{rep}}$ replicas:

$$P = \min\{1, \exp[(\beta_i - \beta_j)(E_i - E_j)]\}. \qquad (3)$$

Here, $i$ and $j$ are the indices of the replicas attempting the swap, and $\beta_{i(j)}$ and $E_{i(j)}$ are the inverse temperatures and energies of each replica. According to this criterion, a replica with lower energy will be assigned progressively lower energies, and vice versa. Essentially, a high-temperature replica is given the task of a global scan of configuration space; when it finds a new local minimum, it will be assigned a lower temperature and will perform a more careful search within the newly found energy basin. In this manner, the RXMC method provides a good balance between global search and local optimization. At the same time, the canonical ensembles are easily recovered by collecting the replicas at each temperature.

Figure 2 shows our computational scheme. There are $N_{\mathrm{rep}}$ Metropolis samplers running at different temperatures; the samplers are coded using python and parallelized using mpi4py [18–20]. At each Metropolis step, each sampler performs a swap between atoms of different types (possibly including vacancies), prepares input files for the specified DFT code, and spawns parallel DFT processes using MPI-2 dynamic process management, i.e., the MPI_COMM_SPAWN function. The DFT

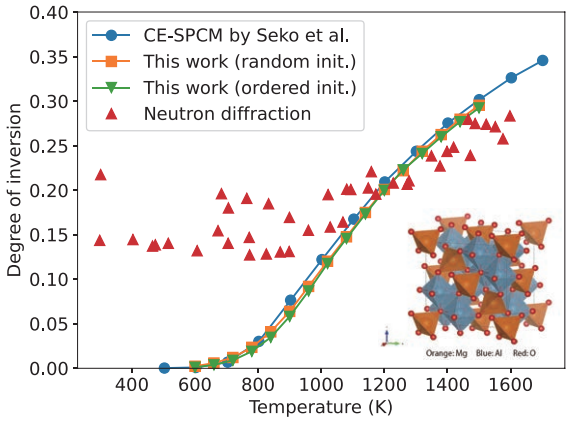


Figure 3: Comparison of the degree of inversion as a function of temperature calculated by CE-SPCM (Seko et al. [21]; circles), the present approach (randomly initialized: squares; initialized with an ordered spinel structure: triangles and experimental neutron diffraction data [22]). The spinel structure is shown in the inset. Reproduced from Ref. [10] with addition of neutron diffraction data.

processes perform local structural relaxation and energy calculation, then the results are read automatically by the sampler to determine whether to accept or reject the new configuration. The samplers also attempt temperature swaps between replicas at preset intervals according to Eq. 3. This multilayered parallelism over replicas and DFT processes makes it ideal for harnessing the power of modern-day parallel supercomputers.

As a first benchmark for testing the feasibility of this approach, we chose to calculate the degree of cation disorder in $MgAl_2O_4$ spinel oxide [10]. Spinel oxides have a general formula of $A(II)B(III)_2O_3$ with A (B) representing a divalent (trivalent) cation, and are of interest in magnetic (spintronic) and electronic applications as well as mineralogy. The structure is shown in Fig. 3. Usually, the divalent cation occupies the tetrahedral sites and the trivalent cation occupies the octahedral sites. However, some inversion between the sites can occur, and some A(II)–B(III) combinations are known to exhibit completely inverse ordering, where all trivalent cations occupy the octahedral sites. The degree of inversion (DOI) is quantified by the ratio of divalent cations at octahedral sites. Seko and coworkers have performed calculations of the DOI in several spinels using cluster expansion [4, 21], and we took their result for $MgAl_2O_4$ as reference. We employed a calculation supercell containing 16 Mg, 32 Al, and 64 O atoms, and sampled the configuration of Mg and Al on the cation sublattice. No disorder on the O sublattice was considered. We performed two separate RXMC runs to check for convergence and initial configuration dependence; one run was initialized with random configurations and another was initialized from the ordered spinel configuration. We used 16 replicas spaced evenly between 600 and 1500 K and performed 16750 steps for the randomly initialized run and 13000 steps for the run initialized from the ordered configuration. This amounts to roughly 4000 node hours for each run on System C (enaga) at ISSP which has two Xeon Gold 6148 processors per node. Figure 3 compares the calculated DOI vs. temperature for the two runs as well as that obtained by a cluster expansion model augmented by a screened point charge model. We find the results to be virtually identical, showing that sufficient sampling steps were performed and it is indeed feasible to perform such calculations on meaningfully large supercells without resorting to fitted models. Moreover, the RXMC calculation initialized in the random configuration discovered the ground state ordered spinel configuration within 300 steps. We think this is rather impressive considering that there are ${}_{48}C_{16} = 2254848913647$ possible configurations, and attests to the efficiency of the RXMC method not only as a sampler but also as an optimizer. We also note that the deviation from experiment at lower temperature is seen in both our calculation and Seko's. This is most likely due to the low mobility of cations at low temperature which inhibits the equilibration in the experiment.

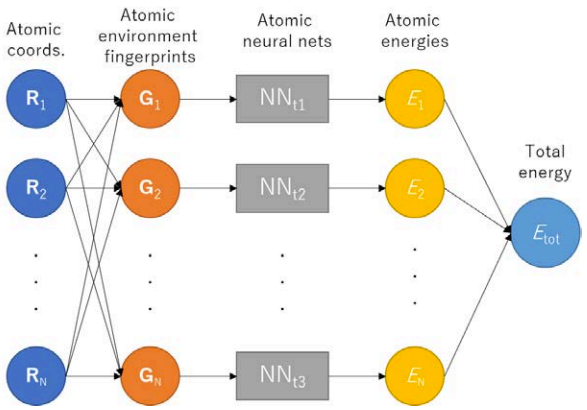


Figure 4: The structure of the HDNNP. The atomic coordinates are converted to a rotationally and translationally invariant environment descriptor before feeding in to the neural network.

## 3 Accelerated sampling utilizing a neural network model combined with active learning [23]

Although direct sampling using DFT-relaxed energies was shown to be feasible as detailed above, the amount of required computer resources is quite large, taking several days to a week to sample just one composition on a modern supercomputer. A much higher throughput is necessary to enable materials design based on such simulations. Also, because of the computational cost of DFT calculations, it is not feasible to go beyond a system size of about one hundred atoms and perform sufficient numbers of sampling steps. This is a problem when treating systems with, e.g., dilute doping or long correlation lengths. To provide the necessary acceleration, we have no choice at this point but to go back to lightweight models. However, as mentioned above, the *de facto* standard cluster expansion approach has difficulty handling complex multicomponent systems that are of interest for various applications.

To overcome this issue, we turned to the high-dimensional neural network potential (HDNNP) approach pioneered by Behler and Parinello [24, 25]. This approach relies on the ansatz that the total energy can be expressed as a sum of atomic energies determined by the environment around each atom and uses a a feed-forward neural network to represent those atomic energies (Fig. 4). The network weights are trained to reproduce DFT energies and forces (i.e., energy derivatives). Acceleration by 2–4 orders of magnitude compared to DFT has been achieved while maintaining similar levels of accuracy.

The HDNNP approach was developed for accelerating molecular dynamics simulations. There, it is necessary to accurately reproduce the energy and forces in continuous coordinate space. This is overkill when considering the lattice configuration problem; we only need to map the ideal lattice structure with configurational disorder to the energy after local relaxation. Thus, we proposed to train the HDNNP model to predict the relaxed energies from the set of atom coordinates and atom species on the ideal lattice [23]. The new ansatz here is that the total energy of a *relaxed* configuration can be expressed as a sum of atomic energies determined from atom environment descriptors calculated on the ideal lattice *before relaxation*. This may be expressed as follows:

$$E_{\mathrm{rel}}(\vec{\sigma}) = \sum_{i}^{\mathrm{atoms}} \mathrm{NNP}^{\mathrm{rel}}_{t_i}(f[\vec{\sigma}_i^{R_c}]) \text{ for } \vec{\sigma} \in \{\vec{\sigma}_{\mathrm{lattice}}\}, \tag{4}$$

where $\vec{\sigma}$ represents the coordinates of all atoms in the system, which is restricted, in our scheme, to those on the ideal lattice. $i$ represents atom indices, $t_i$ is the corresponding atom type, and $\vec{\sigma}_i^{R_c}$ represents the configuration of atoms within a cutoff radius from atom $i$. A separate neural net $\mathrm{NNP}_{t_i}$ is trained for each atom type; it takes as input a rotationally and translationally invariant fingerprint of the atomic environment $f[\vec{\sigma}_i^{R_c}]$ and outputs the contribution of the atom $i$ to the *relaxed* total energy. In this work, we employed the Chebychev fingerprint proposed by Artrith and coworkers [26]. In this fingerprinting scheme, Chebychev expansion coefficients of the radial and angular distribution functions are used as the fingerprint. The atom type is encoded by multiplying with type-dependent factors when calculating the radial/angular distributions. We use ænet code

(`http://ann.atomistic.net/`) for the training and evaluation of the neural network model.

An issue with neural network approaches in general is that they are good at interpolating between training data but not at extrapolating. To overcome this problem, we adopted the so-called "active learning" approach, where the neural network is retrained on-the-fly when the simulation wanders into regions of structure space that were not included in the original training data set [27–35]. Our approach is summarized as follows:

1. Prepare a training set consisting of DFT-relaxed energies of randomly generated configurations.

2. Perform neural network training.

3. Perform RXMC sampling using the trained neural network model.

4. Perform DFT relaxations on a subset of configurations that appeared during RXMC sampling and check the prediction accuracy. If sufficient accuracy is achieved, stop here.

5. If the accuracy is found to be insufficient, add those configurations to the training set and repeat from step 2.

We benchmarked this approach, again, on the temperature dependence of the DOI in $MgAl_2O_4$. We used a supercell with 192 cation sites compared to 48 in the previous section. The supercell size combined with the explosion of the possible number of configurations ($_{192}C_{64} \sim 10^{51}$) makes this calculation completely out of reach for direct sampling on DFT energies.

Figure 5 shows the correlation plot between the neural network predictions vs. reference DFT energies. The model trained on randomly generated configurations performs well in the high energy region but shows a sizable deviation at lower energies. This is because the lower energy structures with more ordering were obviously not included in the original training data set. In our active learning scheme, these structures are then added to the training set and the model is retrained. The resulting correlation after active learning is nearly perfect with deviations of less than a few meV/atom. The active-learned neural network model was used to sample the DOI vs. temperature (Fig. 6) from 480,000 RXMC steps with 15 replicas, and good agreement was obtained with cluster expansion and direct sampling on DFT energies explained in the previous section.

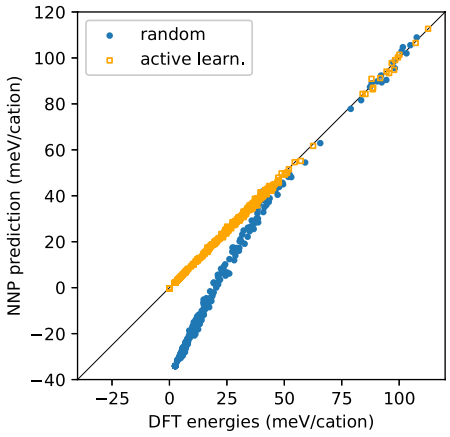


Figure 5: The correlation between reference DFT energies and neural network predictions when training was performed on randomly generated configurations (closed circles) and after performing active learning (open squares).

# 4 Applications

We have only just started to apply the thermodynamic sampling methods outlined in previous sections to complex oxide systems that were difficult to treat using previously available methods. Here, we briefly present some results obtained for a couple of systems of interest in solid state ionics and electrochemistry.

## Acceptor-doped $BaZrO_3$

Ceramic-based electrolytes are under intense research for application in battery, fuel cell, and electrolyzer applications. Recently, we have been focusing on acceptor-doped $BaZrO_3$, which is known as a promising material to be used as the

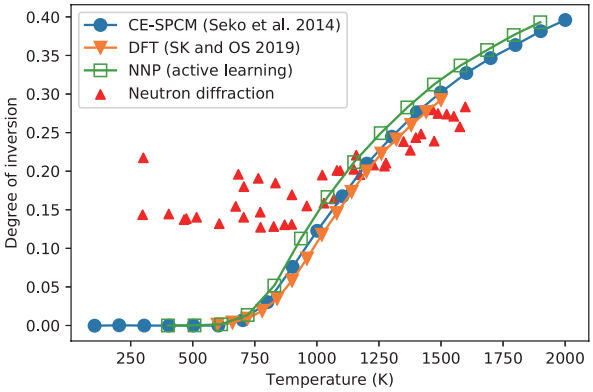


Figure 6: Comparison of the DOI calculated using cluster expansion (blue circles), direct sampling on DFT energies (orange triangles), and the neural network model (open green squares) compared to experiment (red triangles).

proton conducting electrolyte in solid oxide fuel cells. The material is an insulator without doping, but oxygen vacancies with an effective charge of +2 can be induced by substituting $Zr^{4+}$ by trivalent acceptor cations such as $Y^{3+}$. This is expressed in Kröger-Vink notation as follows:

$$2Zr_{Zr}^{\times} + O_O^{\times} + Y_2O_3 \rightarrow 2Y'_{Zr} + V_O^{\bullet\bullet} + 2ZrO_2. \quad (5)$$

These oxygen vacancies are immobile in the temperature range of interest, but highly mobile protons can be induced by a hydration reaction with these vacancies:

$$H_2O + V_O^{\bullet\bullet} + O_O^{\times} \rightarrow 2(OH_O^{\bullet}). \quad (6)$$

The maximum dopant concentration can reach up to 60% depending on the dopant species [36] (although it may be questionable whether it is appropriate to refer to such high concentrations as "doping"). Conventionally, dopants were assumed to distribute randomly on the Zr sites. On the other hand, some recent works have pointed out that the configuration of dopants can impact the proton mobility in both positive and negative ways [37–39]. For example, an isolated dopant or a cluster of dopants can act as a trapping site for protons due to coulomb attraction. On the other hand, dopants may form a long-range percolating pathway along which protons can diffuse relatively freely. Thus, we performed RXMC sampling combined directly with DFT for revealing what the realistic dopant configurations will be under processing conditions in Y-doped $BaZrO_3$ with dopant concentration up to 30%. We note that many works have discussed the interaction between few dopants and O vacancies or protons, but none have treated such highly doped systems rigorously within a statistical thermodynamics framework like ours. Our approach revealed that the dopant configurations are far from random even at the usual sintering temperature of $\sim$ 1800 K. This originates from complex many-body interactions that cannot be explained simply in terms of coulomb interactions between charged defects. Detailed analysis based on the statistics obtained from RXMC samples can be found in Ref. [40]. We also fed the obtained configurations into a master equation model for proton diffusion [41] and found that the realistic dopant configurations obtained by RXMC sampling predicts slightly higher conductivities compared to random configurations [42]. Another insight obtained there is that in general, the formation of deep trapping sites due to dopant clustering has much more profound effect than the formation of a percolating pathway. Thus, avoiding dopant clustering would be the route to higher conductivity in this system.

We are now performing the active learning NN-RXMC approach of Sec. 3 to understand the hydration behavior and the recently reported high conductivity of 0.01 S/cm at 400 °C in 60% Sc-doped $BaZrO_3$ [36]. Prior to this report, Y doping of $\sim$ 20% was reported to result in the highest proton conductivity using $BaZrO_3$ as the parent material. An issue was that further doping results in the decline of proton conductivity, which was also reproduced by our work mentioned above [42]. In the case of Sc, however, the conductivity continues to increase up to 60% doping, which is the solubility limit for this system. It will be interesting and insightful to see how the character of different dopants with the same formal charge can lead to such different behavior. We are working to contribute in this regard using *ab initio* thermodynam-

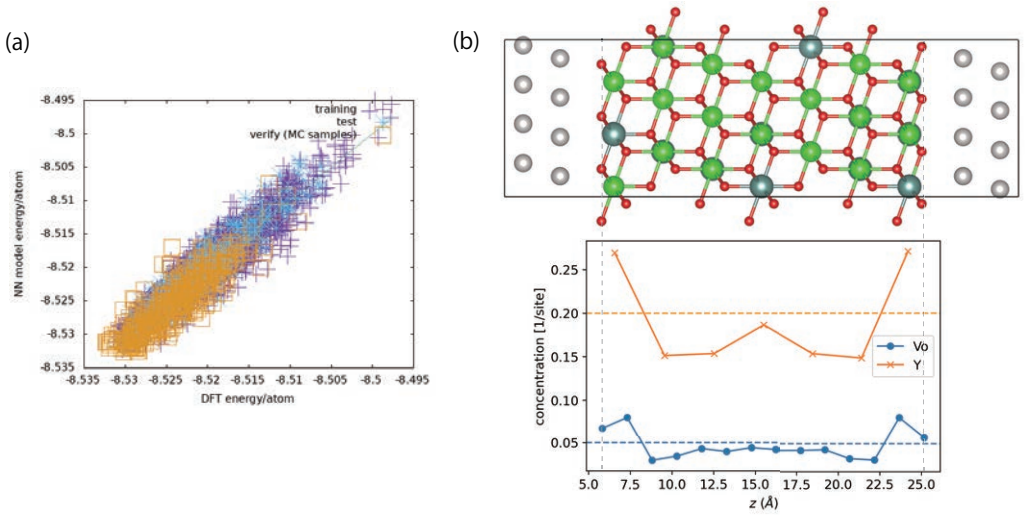


Figure 7: (a) Evaluation of NN accuracy after active learning on The Pt/YSZ slab model and (b) the obtained Y and O vacancy concentration profiles.

ics.

## The ionic space charge layer

Another issue we are currently working on is the ionic space charge effect at solid-solid interfaces. The space charge concept is a central idea of semiconductor device physics, where a depletion or accumulation of holes or electrons occurs to align the Fermi level across the interface. The concept should naturally be extended to mobile ions, which are abundant in solid electrolytes, but the situation is now much more complicated because various ionic species can contribute to the effect, and ions can even be introduced spontaneously (e.g., hydrogen in the atmosphere can spontaneously dope oxides [43]). A related (or maybe equivalent) concept in electrochemistry of liquid electrolytes is the electrical double layer. The nanoscale atomistic details of the space charge layer is expected to modify the ion dynamics in various ways. It should impact the performance of solid state electrochemical devices such as solid-state batteries, fuel cells, and electrolyzers, or may even lead to novel functionalities. Because of this, the topic is under intense study from both experimental and theoretical standpoints (see, e.g., `https://interface-ionics.jp/en/index.html`).

In the past, we have combined ion defect formation energetics calculated using DFT with a Poisson-Boltzmann type model to calculate the ion distribution near metal/solid electrolyte interfaces [44–46]. However, the energetics were calculated in the bulk and do not include effects such as the chemical characteristics of the interface or the concentration dependencies of the dielectric constant. Also, the interactions between defects were modeled considering only ideal point charge electrostatics. In other words, it is a mean field model with many assumptions and may not be reliable enough for certain cases.

*ab initio* statistical thermodynamics approaches introduced above are ideal for tackling this issue and going beyond the simple mean-field picture. As a first step, we calculated the ion distribution in the Pt (111)/Yttria-stabilized zirconia (YSZ) (111) slab model (Fig. 7). Note that YSZ is a well-studied oxide ion conductor for application in solid oxide fuel cells. The parent lattice is cubic fluorite $ZrO_2$ with 68 Zr sites and 126 O sites, and configurations of 12 Y ions on Zr sites and 6 O vacancies residing on the O sites were sampled using our active learning NN-RXMC approach (Sec. 3). The correlation between the DFT energies and NN predictions of the training, test, and verification sets

seems to be good enough, although not as perfect as the bulk $MgAl_2O_4$ case (Fig. 5). The calculated concentration profiles show a segregation of Y on the outermost Zr layer and depletion on the second and third Zr layers. There is also an increase in the vacancy concentration on the second O layer. The next challenge would be to consider variations in the number of oxygen vacancies and perform grand canonical sampling, so that the results can be compared directly with experiments which control the oxygen partial pressure. We expect these calculations to be immensely useful for understanding the thermodynamics of space charge layer formation, and also to serve as a basis for understanding the modification of various materials properties due to formation of interfaces.

# 5 ab Initio Configuration Sampling Toolkit (abICS)

The software framework for direct coupling of RXMC sampling with DFT (Sec. 2) was selected as an ISSP Project for Advancement of Software Usability in Materials Science for SY2019. Parts of the prototype code developed by the author (S.K.) were rewritten in modular fashion so as to enable easy extension of the framework. The original prototype only supported VASP as the energy calculator, but interfaces for OpenMX and Quantum Espresso are now supported. In addition, a user interface employing the human-readable and computer-friendly TOML format (`https://toml.io/en/`) was developed for setting up the calculations. The code has been named ab Initio Configuration Sampling Toolkit, or *abICS* for short, and released to the public under an open source license (GPL ver. 3), along with a user manual. It is under continous development (`https://www.pasums.issp.u-tokyo.ac.jp/abics/`, `https://github.com/issp-center-dev/abICS`), and we are in the process of implementing the active learning approach explained in Sec. 3.

# 6 Summary and outlook

In this report, we presented our recent efforts in enabling configurational sampling in complex oxide systems from first principles. By harnessing the power of modern day supercomputers in combination with extended ensemble sampling, it has now become just barely feasible to perform sampling directly on DFT energies on unit cells of $\sim$ 100 atoms. We also demonstrated that similar accuracy can be achieved with a speedup by a factor of $\sim 10^4$ by the use of a neural network model that reproduces the configuration energetics. This has made possible routine sampling on unit cells of a few hundred atoms with *ab initio* accuracy.

We have been implementing these approaches in an open source framework *abICS*. We believe that this framework will be immensely useful for making efficient use of the ever-increasing capacity of modern supercomputers. We are also aiming to bring together information science, materials simulation, and statistical physics using *abICS* as a hub. Because of modular coding practices employed in our project, it should be relatively easy to implement interfaces for other solvers, or to implement new sampling schemes. Please and do not refrain from contacting us if you are interested in using or extending this software.

# Acknowledgements

*abICS* is developed by Yuichi Motoyama, Kazuyoshi Yoshimi, Yoshiyuki Yamamoto, Osamu Sugino, Taisuke Ozaki, and the author (S.K.) as part of the ISSP Project for Advancement of Software Usability in Materials Science. The calculations presented in this work were performed on the ISSP Joint-Use Supercomputer Systems “sekirei”, “enaga”, and “ohtaka” as well as on the supercomputer Fugaku provided by RIKEN for the Fugaku Battery and Fuel Cell Project. This report reviewed works supported over the years by KAKENHI (Grant numbers JP18H05519, 19K15287, 20H05284), MEXT LEADER program, and JST CREST (JPMJCR15Q3) and

FOREST (JPMJFR2037) programs. Atomic structure figures were drawn using VESTA [47].

## References


[1] J. M. Sanchez, F. Ducastelle, and D. Gratias, Physica A **128A**, 334 (1984).

[2] G. Ceder, Comput. Mater. Sci. **1**, 144 (1993).

[3] A. van de Walle, M. Asta, and G. Ceder, Calphad **26**, 539 (2002).

[4] A. Seko, Y. Koyama, and I. Tanaka, Phys. Rev. B **80**, 165122 (2009).

[5] J. M. Sanchez, Phys. Rev. B **81**, 224202 (2010).

[6] J. M. Sanchez, J. Phase Equilib. Diffus. **38**, 238 (2017).

[7] Q. Wu, B. He, T. Song, J. Gao, and S. Shi, Comput. Mater. Sci. **125**, 243 (2016).

[8] J. H. Chang, D. Kleiven, M. Melander, J. Akola, J. M. Garcia-Lastra, and T. Vegge, J. Phys.: Condens. Matter **31**, 325901 (2019).

[9] K. Yuge, A. Seko, A. Kuwabara, F. Oba, and I. Tanaka, Phys. Rev. B **76**, 045407 (2007).

[10] S. Kasamatsu and O. Sugino, J. Phys.: Condens. Matter **31**, 085901 (2019).

[11] J. Jellinek, S. Srinivas, and P. Fantucci, Chem. Phys. Lett. **288**, 705 (1998).

[12] S. Wang, S. J. Mitchell, and P. A. Rikvold, Comput. Mater. Sci. **29**, 145 (2004).

[13] A. M. Ferrenberg and R. H. Swendsen, Phys. Rev. Lett. **61**, 2635 (1988).

[14] B. A. Berg and T. Neuhaus, Phys. Rev. Lett. **68**, 9 (1992).

[15] F. Wang and D. P. Landau, Phys. Rev. Lett. **86**, 2050 (2001).

[16] S. N. Khan and M. Eisenbach, Phys. Rev. B **93**, 024203 (2016).

[17] K. Hukushima and K. Nemoto, J. Phys. Soc. Jpn. **65**, 1604 (1996).

[18] L. Dalcín, R. Paz, and M. Storti, J. Parallel Distrib. Comput. **65**, 1108 (2005).

[19] L. Dalcín, R. Paz, M. Storti, and J. D'Elía, J. Parallel Distrib. Comput. **68**, 655 (2008).

[20] L. D. Dalcin, R. R. Paz, P. A. Kler, and A. Cosimo, Adv. Water Resour. **34**, 1124 (2011).

[21] A. Seko and I. Tanaka, J. Phys.: Condens. Matter **26**, 115403 (2014).

[22] S. A. T. Redfern, R. J. Harrison, H. S. C. O'Neill, and D. R. R. Wood, Am. Mineral. **84**, 12 (1999).

[23] S. Kasamatsu, Y. Motoyama, K. Yoshimi, U. Matsumoto, A. Kuwabara, and T. Ogawa, (2020), arXiv preprint: 2008.02572.

[24] J. Behler, Int. J. Quantum Chem. **115**, 1032 (2015).

[25] S. Watanabe, W. Li, W. Jeong, D. Lee, K. Shimizu, E. Mimanitani, Y. Ando, and S. Han, J. Phys.: Energy **3**, 012003 (2020).

[26] N. Artrith, A. Urban, and G. Ceder, Phys. Rev. B **96**, 014112 (2017).

[27] E. V. Podryabinkin and A. V. Shapeev, Comput. Mater. Sci. **140**, 171 (2017).

[28] E. V. Podryabinkin, E. V. Tikhonov, A. V. Shapeev, and A. R. Oganov, Phys. Rev. B **99**, 064114 (2019).

[29] K. Gubaev, E. V. Podryabinkin, G. L. Hart, and A. V. Shapeev, Comput. Mater. Sci. **156**, 148 (2019).

[30] J. S. Smith, B. Nebgen, N. Lubbers, O. Isayev, and A. E. Roitberg, J. Chem. Phys. **148**, 241733 (2018).

[31] L. Zhang, D.-Y. Lin, H. Wang, R. Car, and W. E, Phys. Rev. Mater. **3**, 023804 (2019).

[32] T. Kostiuchenko, F. Körmann, J. Neugebauer, and A. Shapeev, npj Comput. Mater. **5**, 1 (2019).

[33] T. D. Loeffler, T. K. Patra, H. Chan, M. Cherukara, and S. K. R. S. Sankaranarayanan, J. Phys. Chem. C **124**, 4907 (2020).

[34] J. Vandermause, S. B. Torrisi, S. Batzner, Y. Xie, L. Sun, A. M. Kolpak, and B. Kozinsky, npj Comput. Mater. **6**, 20 (2020).

[35] R. Jinnouchi, K. Miwa, F. Karsai, G. Kresse, and R. Asahi, J. Phys. Chem. Lett. **11**, 6946 (2020).

[36] J. Hyodo, K. Kitabayashi, K. Hoshino, Y. Okuyama, and Y. Yamazaki, Adv. Energy Mater. **n/a**, 2000213 (2020).

[37] K. Toyoura, W. Meng, D. Han, and T. Uda, J. Mater. Chem. A **6**, 22721 (2018).

[38] K. Toyoura, T. Fujii, N. Hatada, D. Han, and T. Uda, J. Phys. Chem. C **123**, 26823 (2019).

[39] F. M. Draber, C. Ader, J. P. Arnold, S. Eisele, S. Grieshammer, S. Yamaguchi, and M. Martin, Nature Mater. (2019).

[40] S. Kasamatsu, O. Sugino, T. Ogawa, and A. Kuwabara, J. Mater. Chem. A **8**, 12674 (2020).

[41] K. Toyoura, T. Fujii, N. Hatada, D. Han, and T. Uda, J. Phys. Chem. C **123**, 26823 (2019).

[42] T. Fujii, K. Toyoura, T. Uda, and S. Kasamatsu, Phys. Chem. Chem. Phys. **23**, 5908 (2021).

[43] C. G. Van de Walle, Phys. Rev. Lett. **85**, 1012 (2000).

[44] S. Kasamatsu, T. Tada, and S. Watanabe, Solid State Ionics **183**, 20 (2011).

[45] S. Kasamatsu, T. Tada, and S. Watanabe, Solid State Ionics **226**, 62 (2012).

[46] K. Shimizu, W. Liu, W. Li, S. Kasamatsu, Y. Ando, E. Minamitani, and S. Watanabe, Phys. Rev. Mater. **4**, 015402 (2020).

[47] K. Momma and F. Izumi, J. Appl. Crystallogr. **41**, 653 (2008).